ORIGINAL SCIENTIFIC PAPER

CROATICA CHEMICA ACTA

Croat. Chem. Acta **2022**, *95*(2), 57–68
Published online: February 17, 2023
DOI: 10.5562/cca3922

HKD 1926

Molecular Recognition between Anticancer Drug, Regorafenib and Human Serum Albumin: Interaction Revisited

Salanee Kandandapani,[1] Md. Zahirul Kabir,[1] Hafsa Tayyab,[2] Saharuddin B. Mohamad,[2,3] Saad Tayyab[4,*]

[1] Biochemistry Programme, Institute of Biological Sciences, Faculty of Science, Universiti Malaya, Kuala Lumpur, Malaysia
[2] Bioinformatics Programme, Institute of Biological Sciences, Faculty of Science, Universiti Malaya, Kuala Lumpur, Malaysia
[3] Centre of Research for Computational Sciences and Informatics for Biology, Bioindustry, Environment, Agriculture and Healthcare, Universiti Malaya, Kuala Lumpur, Malaysia
[4] Department of Pharmaceutical Chemistry, Faculty of Pharmaceutical Sciences, UCSI University, Kuala Lumpur, Malaysia
* Corresponding author's e-mail address: Saad.Tayyab@ucsiuniversity.edu.my

RECEIVED: September 20, 2022 * REVISED: December 25, 2022 * ACCEPTED: January 12, 2023

Abstract: The wet-lab techniques (fluorimetry and spectrophotometry), along with computational techniques (molecular docking and molecular dynamics (MD) simulation), were applied to re-examine the association of an anticancer drug, regorafenib (REG) with human serum albumin (HSA). The REG-induced protein fluorescence quenching was characterized as static quenching based on a decrement in the K_{SV} (Stern-Volmer constant) with increasing temperature and hyperchromic effect in the absorption spectra. The REG–HSA complex (K_a = 0.63 – 1.17 × 10^5 M^{-1}) was stabilized by hydrophobic and van der Waals interactions in combination with hydrogen bonds, as revealed by thermodynamic data ($\Delta_r S°$ = +17.17 J mol^{-1} K^{-1} and $\Delta_r H°$ = –23.00 kJ mol^{-1}), and further supported by molecular docking assessment. Microenvironmental fluctuations around HSA fluorophores and better protein stability against thermal stress were evident due to REG-HSA complexation. Accessibility of both Sudlow's Sites I and II but priority for Site I of the protein for REG was inferred by the competitive ligand displacement and molecular docking assessments. MD simulation results supported the stability of the complex.

Keywords: human serum albumin, regorafenib, fluorescence quenching, ligand-protein interaction, molecular dynamics simulations.

INTRODUCTION

REGORAFENIB (REG) (Figure 1.) is a promising, orally-administered inhibitor of multikinases such as VEGFR 1–3, PDGFR β & α, FGFR 1-2, TIE-2, c-Kit, RET, RAF-1, BRAF and MAP kinases. The FDA-authorized drug treats metastatic colorectal cancer and gastrointestinal stromal tumours.[1,2] REG competes with ATP for the ATP-binding site and halts certain subsequent signalling pathways of these kinases liable for cancer progression, thus inhibiting tumour growth.[3,4] Several clinical trials (mostly Phase II) are in progress to develop REG as the potential therapeutic agent in the treatment of various human malignancies, including hepatocellular carcinoma, metastatic renal cell carcinoma, and soft tissue sarcoma.[5] Even though several reports evaluated REG's biological function in human cells,[5–7] information concerning its transportation in human blood plasma has not been revealed.

The delivery of many exogenous ligands, including drugs, to the specific target tissues/organs in human blood plasma is primarily performed by serum albumin (HSA),

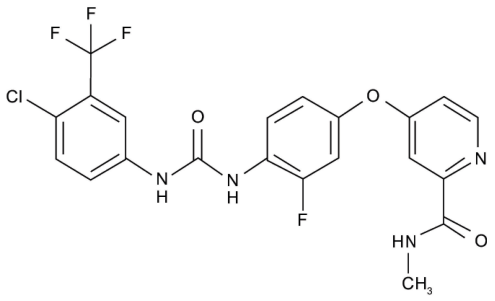

Figure 1. The 2-D structure of REG.

owing to its three well-characterized drug binding sites, *i.e.*, Site I (subdomain IIA), Site II (subdomain IIIA) and Site III (subdomain IB).[8] Ligand-protein association markedly improves the drug's therapeutic and targeting potential, protects them against oxidation, decreases the side effects and alters the pharmacokinetic features in distribution, clearance and elimination across the human system.[9–11]

Although a recent report[12] sheds light on the interaction of REG with HSA using fluorescence and docking methods, it suffers from several drawbacks. Use of an excitation wavelength of 280 nm instead of 295 nm in the titration experiment, describing the mode of static quenching without temperature-dependent titration or absorption spectral data, lacking thermodynamic data to define the binding forces and absence of warfarin-HSA fluorescence to determine Site I involvement are some of the limitations in the published paper.

In this report, we present the interaction characteristics of the REG–HSA system in terms of the affinity, forces and mechanism of the association process and locus of the REG binding site in HSA using fluorescence and absorption spectroscopic techniques in combination with molecular docking and simulation approaches.

EXPERIMENTAL

Reagents

Albumin from human serum (globulin and essential fatty acid-free; purity ≥ 99 %), phenylbutazone (PBZ; purity ≥ 98 %), warfarin (WFN; purity ≥ 98 %) and diazepam (DZM; purity ≥ 98 %) were purchased from Sigma-Aldrich Co., St Louis, MO, USA. Regorafenib (REG; purity ≥ 99.9 %) was supplied by Selleckchem, Houston, TX, USA. Other analytical grade reagents and Milli-Q water (Merck Millipore) were used in these experiments.

Protein and Drug Solutions

The sodium phosphate buffer, 60 mM, pH 7.4 (PB 7.4), was used to prepare the protein solution. REG, WFN, PBZ, and DZM were dissolved (1.0 mg ml^{-1}) in dimethyl sulfoxide (DMSO) and diluted with PB 7.4 per the desired concentration. The protein (ε_m of 36 500 M^{-1} cm^{-1} at 280 nm)[13] and WFN (ε_m = 13 600 M^{-1} cm^{-1} at 310 nm)[14] concentrations were determined spectrophotometrically.

Absorption Spectra

The absorption spectra (240–320 nm) of the protein alone, REG alone and REG-protein mixtures ([HSA] = 15 μmol dm^{-3}, [REG] = 0, 5, 10, 15, 20, 25, 30 μmol dm^{-3}) were registered on a Shimadzu UV-2450 spectrophotometer, using a set of 1 cm quartz cuvettes. For correcting the fluorescence intensity values, absorption spectra (295–390 nm) of HSA (3 μmol dm^{-3}) in the presence of 1, 2, 3, 4, 5 and 6 μmol dm^{-3} of REG were collected.

Fluorescence Spectra

The fluorescence spectra (λ_{ex} = 295 nm, λ_{em} = 310–390 nm) of the protein alone (3 μmol dm^{-3} HSA) and with REG (0, 1, 2, 3, 4, 5 and 6 μmol dm^{-3}) were registered on a Jasco FP-6500 spectrofluorometer using a 10 mm quartz cuvette. The solutions were incubated individually at 288 K, 298 K and 308 K for 30 min to achieve equilibrium, followed by positioning the cuvette in a thermostatically-regulated cell holder for 6 min to equilibrate the sample temperature. As described previously, other scanning parameters were retained the same.[15]

The fluorescence spectra (λ_{ex} = 335 nm, λ_{em} = 360–480 nm) of WFN–protein and WFN–protein–REG mixtures were also recorded.

The three-dimensional (3-D) fluorescence spectra of 3 μmol dm^{-3} protein and 2 : 1 REG–protein mixture were acquired per the published method.[16]

Analysis of Fluorescence Data

The fluorescence intensity values (F_{obs}) were corrected (F_{cor}) for the inner filter effect correction using the following equation:[17]

$$F_{cor} = F_{obs}\, 10^{(A_{ex}+A_{em})/2} \quad (1)$$

where A_{ex} and A_{em} are the changes in the absorbance between the protein and the drug-protein mixtures at the λ_{ex} (295 nm) and the λ_{em} (310–390 nm), respectively.

Equations 2–5 were used to determine various binding parameters *viz.* the Stern-Volmer constant, K_{SV}, and the bimolecular quenching rate constant, k_q (Eq. 2), the binding constant, K_a (Eq. 3), and thermodynamic parameters, *i.e.* the standard reaction enthalpy, $\Delta_r H°$ and the standard reaction entropy, $\Delta_r S°$ (Eq. 4) and the standard reaction Gibbs free energy, $\Delta_r G°$ (Eq. 5) for REG-HSA system. The fluorescence lifetime (τ_0) of the protein without the quencher (REG) was taken as 5.6×10^{-9} s[18] in the k_q calculation using Eq. (2).

$$F_0 / F = K_{SV}[Q] + 1 = k_q \tau_0 [Q] + 1 \quad (2)$$

$$\frac{\log(F_0 - F)}{F} = n\log K_a - n\log\left[\frac{1}{[L_T] - (F_0 - F)[P_T]/F_0}\right] \quad (3)$$

$$\ln K_a = \frac{-\Delta_r H°}{RT} + \frac{\Delta_r S°}{R} \quad (4)$$

$$\Delta_r G° = \Delta_r H° - T\Delta_r S° \quad (5)$$

The individual terms have their standard significance.[16]

Thermal Stability Measurements

The protein's thermostability was assessed in the same way as described earlier[19] by measuring the fluorescence intensity at 343 nm ($FI_{343\ nm}$) of HSA (3 μmol dm^{-3}) and 2 : 1 REG–HSA mixture at increasing temperatures (298–353 K with increments of 5 K).

Influence of Site Markers on REG–HSA Interaction

Identification of the favored REG binding locus on HSA was investigated using different site-specific drug markers, *i.e.*, PBZ and WFN (Site I markers) and DZM (Site II marker).[9] These experiments were carried out by titrating HSA (3 μmol dm^{-3}) or site marker-protein ([WFN]/[PBZ]/[DZM] : [HSA] = 1 : 1; previously incubated for 30 min at 298 K) mixtures with rising REG concentrations (1–6 μmol dm^{-3} with 1 μmol dm^{-3} intervals). These fluorescence spectra were scanned after further incubating the samples for 30 min at 298 K.

Molecular Docking

The crystal structure of the protein (PDB ID: 1BM0; resolution: 2.5 Å) was collected from the Protein Data Bank.[20] The REG 3-D structure (CID: 11167602) was retrieved from the PubChem database in structure-data file (SDF) format.[21] The structure of REG was further converted to PDB format using Open Babel software.[22] The molecular docking of REG to HSA was conducted using AutoDock 4.2 and AutoDockTools 1.5.6.[23] All water molecules were removed from the crystal structure of HSA, polar hydrogen atoms were added to the protein structure, and Kollman united atom partial charges were assigned. Similarly, the Gasteiger charges were computed, and rotatable bonds were determined for REG optimization. The REG was docked separately into two binding sites of the protein, *i.e.*, Site I (x = 35.4, y = 32.4 and z = 36.5) and Site II (x = 14.4, y = 23.6, z = 23.3) with a grid of 70 × 70 × 70 points and grid spacing of 0.375 Å. The Lamarckian genetic algorithm was employed for conformational searching with 150 population size, 27,000 generations, 250,000 energy evaluations, 0.02 mutation rate, 0.8 crossover rate and 1 elitism.[24] The REG docking modes were clustered according to the root-mean-square-deviation (RMSD) cutoff at 2.0 Å. The UCSF Chimera 1.13.1[25] was utilized to visualise the REG–protein complex. Furthermore, two-dimensional interaction maps between REG and the protein's binding sites were retrieved using LigPlot+.[26]

Molecular Dynamics (MD) Simulation

The ligand-protein complex with bound REG at Site I was subjected to an MD simulation for 50 ns duration using GROMACS 5.0.4 freeware.[27] The topologies of HSA and REG were generated through the CHARMM36 force field[28] and the SwissParam tool[29], respectively, while the cubical box with a 1 nm distance was solvated using the TIP3P water model.[30] Neutralization of the solvated system was done by adding 15 Na^+ ions, followed by energy minimization to remove steric clashes using the steepest descent method for 50,000 steps. The equilibration run for the NVT and NPT ensembles was carried out on a 0.5 ns time scale. During the 50 ns production run, the pressure at 1.0 bar and the temperature at 300 K were kept constant using the Langevin thermostat and piston methods.[31] The Particle Mesh Ewald (PME) method[32] and LINear Constraint Solver (LINCS) algorithm[33] were used for calculating the long-range electrostatic interactions and controlling the bond lengths of hydrogen atoms, respectively. Finally, GROMACS packages and GRACE 5.1.22 program were used to analyze the MD trajectory.[34]

Statistical Analysis

The obtained physical properties characterizing the REG–HSA interaction in solution were converted into the mean ± standard deviation (SD) based on the average value of three separate experiments with the help of the following formula:

$$\sigma = \sqrt{\frac{1}{N}\sum_{i=1}^{N}(x_i - \mu)^2} \qquad (6)$$

where N is the total number of values, x_i is an individual value and μ is the mean value. Statistical data processing and curve fitting, including smoothing, were done by exploiting the OriginPro 8.5 software (OriginLab Corp., Northampton, USA).

RESULTS AND DISCUSSION

Fluorescence Spectra and Quenching Mechanism of the REG–HSA System

Fluorescence spectroscopy is a sensitive, simple and convenient method for studying the ligand-protein interaction and protein conformation. Protein fluorescence mainly originates from tryptophan (Trp) due to its dominance over the other two aromatic amino acids (Tyr and Phe)[17]. The fluorescence of the protein, excited at 295 nm or 280 nm, arises from only Trp or both Trp and Tyr residues. Moreover, compared to 280 nm, the relatively long excitation wavelength (295 nm) avoids energy transfer from Tyr to Trp and prevents inter-tryptophyl transfer.[35] Since HSA contains a single Trp residue in subdomain IIA (Site I), we performed the fluorescence quenching titration experiments of HSA with REG at 295 nm to directly monitor the changes around this site.

Microenvironmental variations around Trp of the protein upon ligand binding usually result in modulation in the protein's fluorescence characteristics. Various molecular

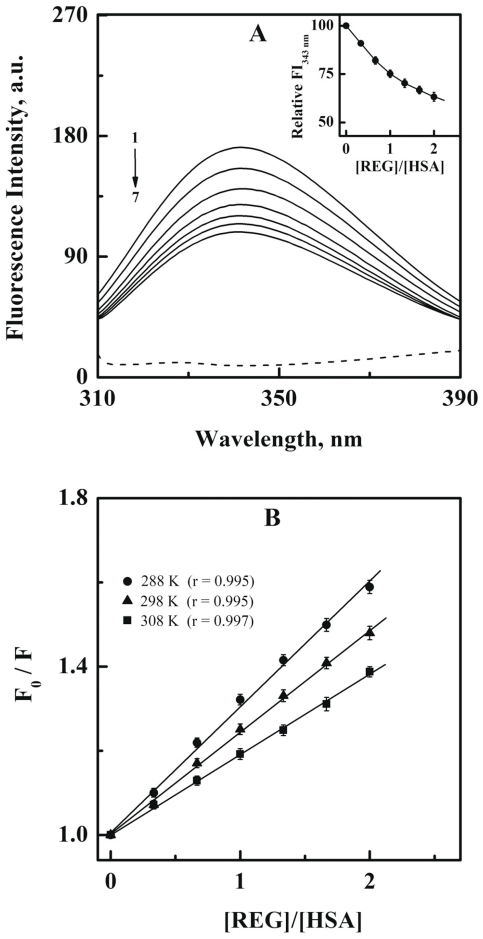

Figure 2. (A) REG-induced fluorescence quenching results of HSA (3 μmol dm^{-3}) with the inclusion of rising (0, 1, 2, 3, 4, 5 and 6 μmol dm^{-3}) REG concentrations (spectra' 1' to '7'), obtained in PB 7.4 at 298 K. The REG (6 μmol dm^{-3}) fluorescence spectrum is marked with a dashed line. The decline in the fluorescence intensity value at 343 nm ($FI_{343\ nm}$) of HSA with rising REG/HSA molar ratios is presented in the inset of Figure (A). (B) Stern-Volmer plots for REG–HSA system, as obtained from REG-induced fluorescence quenching results of the protein at 288, 298 and 308 K.

phenomena, *viz*. excited state reactions, ground-state complex formation, molecular rearrangements, energy transfer and collisional quenching, have been proposed to be accountable for such effects.[17] Fluorescence spectra of HSA alone and with the inclusion of rising REG concentrations are presented in Figure 2A. The protein's fluorescence spectrum exhibited an emission peak (λ_{em}) at 343 nm owing to the existence of the Trp residue in the protein. The addition of increasing concentrations of REG triggered a gradual loss in the fluorescence intensity of HSA, showing a ~37 % decline in the fluorescence intensity value (inset of Figure 2A.) along with a 2 nm blue shift in the λ_{em} at the REG/HSA molar ratio of 2 : 1. The charged groups' movement and hydrophobic microenvironment changes around fluorophores are responsible for decreasing the fluorescence intensity.[36] Such fluctuations in the fluorescence features demonstrated variations in the microenvironmental polarity around Trp upon REG-HSA complexation. It may be noted that REG alone was devoid of any fluorescence intensity in this wavelength range (Figure 2A.).

The mechanism of the protein fluorescence quenching can be categorized as either dynamic or static quenching, which can be differentiated from each other based on their temperature dependence. Rising temperatures lead to the separation of weakly-bound complexes, hence declining the K_{SV} value in static quenching. In contrast, a greater diffusion coefficient with growing temperature raises the K_{SV} value in dynamic quenching.[17,37,38] Titrations and evaluations were carried out at temperatures 288, 298 and 308 K (Supplementary Figure 1.) to speculate on the quenching mechanism associated with the REG–HSA system using Eq. 2. The generated Stern-Volmer plots are presented in Figure 2B., whereas the K_{SV} values, as realized from the slope of these plots, are registered in Table 1. Reduction in the K_{SV} value with increasing temperature (Table 1) for REG–HSA system pointed out a static quenching mechanism for the REG-HSA system, corroborating the complexation between REG and the protein. Additionally, the calculated values of k_q (1.80×10^{13}, 1.46×10^{13} and 1.14×10^{13} M^{-1} s^{-1} at 288, 298 and 308 K, respectively) were significantly larger than the value (2×10^{10} M^{-1} s^{-1}) for the highest dynamic quenching rate constant, reported for the diffusion-controlled process.[39] This also suggested that the fluorescence quenching of HSA was initiated by complex formation between REG and HSA.

Table 1. Binding constants and thermodynamic parameters for REG–HSA interaction at three different temperatures in PB 7.4.

T / K	$K_{sv} \times 10^5$ / M^{-1}	$K_a \times 10^5$ / M^{-1}	$\Delta_r S°$ / J mol^{-1} K^{-1}	$\Delta_r H°$ / kJ mol^{-1}	$\Delta_r G°$ / kJ mol^{-1}
288	1.01 ± 0.07	1.17 ± 0.11			– 27.94 ± 0.06
298	0.82 ± 0.10	0.85 ± 0.09	+ 17.17 ± 0.13	– 23.00 ± 0.12	– 28.11 ± 0.08
308	0.64 ± 0.09	0.63 ± 0.08			– 28.28 ± 0.07

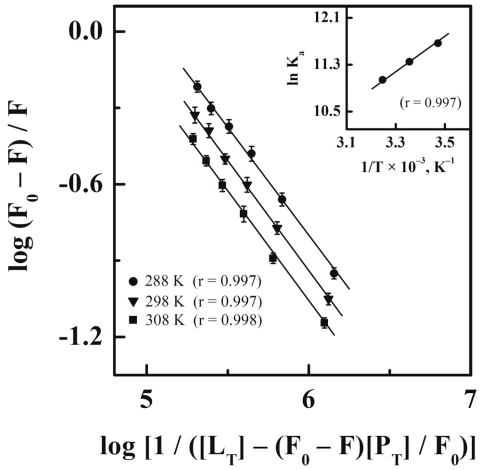

Figure 3. Double logarithmic plots for the REG-HSA system, as attained from REG-induced fluorescence quenching results of HSA at 288, 298, and 308 K. Inset depicts the van't Hoff plot for the REG-HSA system.

Binding Characteristics and Thermodynamics of the REG–HSA System

The K_a values for REG-protein interaction at different temperatures (Table 1) were determined from the double logarithmic plots (Figure 3.) using Eq. 3. The values of K_a were seen to fall in the order of 10^5 (K_a = 0.63–1.17 × 10^5 M^{-1}), suggestive of intermediate binding affinity between REG and the protein. Such binding strength appears suitable for the active transport of REG in the blood plasma and its successive discharge at the target location in the body. Numerous therapeutic drugs have been shown to bind proteins with intermediate binding affinity.[40–44] Furthermore, a decline in the K_a value with rising temperature suggested destabilization of the REG-protein complex with increasing temperature[45–47]

Quantitative evaluation of the energetics of ligand-protein interaction is crucial as it provides valuable information regarding binding forces such as hydrogen bonds, electrostatic, hydrophobic and van der walls forces.[48] Analysis of the temperature dependence of the K_a values using Eq. 4 yielded the van't Hoff plot (inset of Figure 3.) to depict the acting forces that participated in REG–HSA interaction. The values of $\Delta_r H°$ and $\Delta_r S°$ of the association process were attained from the slope and intercept, respectively, of the van't Hoff plot. In contrast, the replacement of $\Delta_r H°$ and $\Delta_r S°$ values in Eq. 5 resulted in the values of $\Delta_r G°$. Table 1. represents $\Delta_r H°$, $\Delta_r S°$ and $\Delta_r G°$ values for REG–HSA interaction. The interaction process between REG and HSA seemed favourable at all three temperatures, as guided by the negative $\Delta_r G°$ values. The negative $\Delta_r H°$ value projected the participation of van der Waals interactions and hydrogen bonds in REG–protein interaction. However, the positive $\Delta_r S°$ value indicated the contribution of electrostatic and hydrophobic interactions.[49] However, electrostatic interactions are typically succeeded by a small $\Delta_r H°$ value (close to zero).[49] Thus, the large negative value (– 23.00 kJ mol^{-1}) of $\Delta_r H°$ in the REG–HSA complexation ruled out the involvement of electrostatic interactions. Considering the possibility of several interactions in the REG–HSA, it would be inconceivable to assume the involvement of a single binding force in the interaction. Therefore, hydrophobic interactions, van der Waals interactions and hydrogen bonds are believed to collectively contribute to the overall energetics of the REG–HSA interaction. The molecular docking assessment also supported the participation of these non-covalent interactions in the REG binding to HSA.

Absorption Spectral Results of the REG–HSA System

Ultraviolet-visible (UV-vis) absorption spectra of the protein with and without ligand have also been used to characterize the mechanism of protein fluorescence quenching.[50] Figure 4. exhibits the absorption spectra of HSA alone and with the addition of REG concentrations (5, 10, 15, 20, 25, and 30 µmol dm^{-3}). These spectra were attained after subtracting the absorption contribution of pure REG (Supplementary Figure 2B.) from the absorption values of respective REG–HSA mixtures (Supplementary Figure 2A.). The emergence of an absorption peak

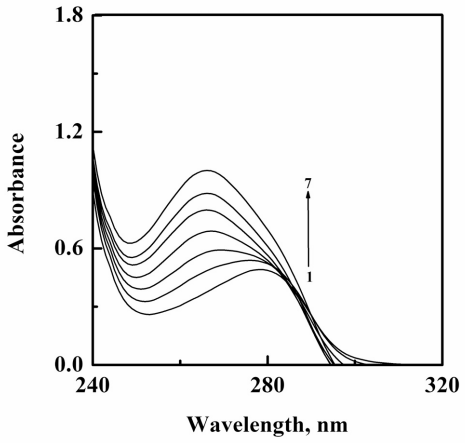

Figure 4. Changes in the absorption spectrum of 15 µmol dm^{-3} HSA (spectrum '1') upon inclusion of rising (5, 10, 15, 20, 25, and 30 µmol dm^{-3}) REG concentrations (spectra' 2–7'), as acquired in PB 7.4 at 298 K. These spectra were acquired by deducting the absorption contribution of pure REG from the absorption spectra of REG–protein mixtures, as presented in Supplementary Figure 2.

Table 2. Spectral characteristics of the 3-D fluorescence spectra of the protein (HSA, 3 μmol dm^{-3}) and REG:HSA mixture in a molar ratio of 2:1, as obtained in PB 7.4 at 298 K.

System	Peak	Peak position (λ_{ex} / nm) / (λ_{em} / nm)	Intensity
HSA	a	230/230 → 350/350	20.2 → 67.3
	b	250/500	65.0
	1	280/338	300.7
	2	230/335	111.5
[REG]:[HSA] = 2:1	a	230/230 → 350/350	21.8 → 218.6
	b	250/500	79.4
	1	280/337	216.5
	2	230/335	45.7

(spectrum 1) at 280 nm was ascribed to the existence of the protein's chromophores, *i.e.,* Trp and Tyr residues in HSA.[51,52] Added REG (spectra 2–7) to the HSA sample produced detectable hypsochromic-hyperchromic shift, which manifested microenvironmental fluctuations around Trp and Tyr residues owing to REG binding to HSA. These results suggested the REG–protein complexation and further supported our fluorescence quenching titration findings.

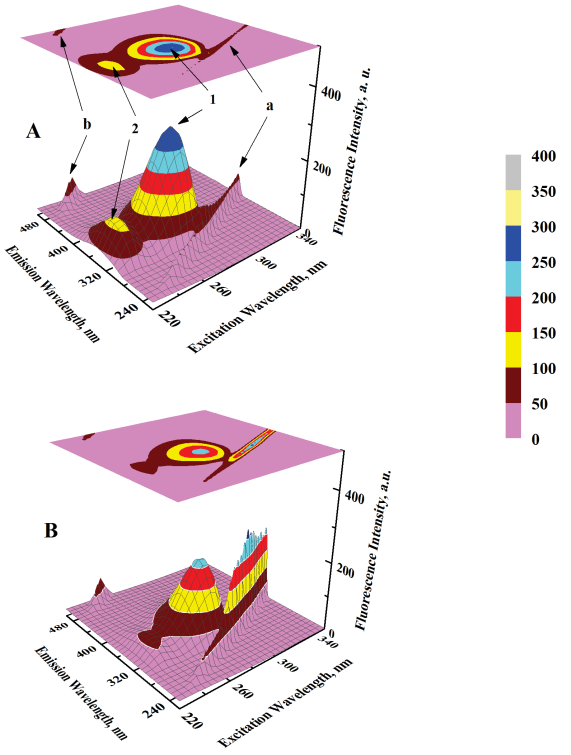

Figure 5. The 3-D fluorescence spectra with top contour maps of (A) 3 μmol dm^{-3} HSA and (B) REG : HSA mixture in a molar ratio of 2 : 1, as obtained in PB 7.4 at 298 K.

Three-Dimensional Fluorescence Spectral Results of the REG–HSA System

To monitor alteration in the Trp / Tyr surroundings in the protein with the inclusion of REG, the 3-D fluorescence spectra of the protein and 2 : 1 REG-protein mixture were registered. These spectra, along with their (top) contour maps, are presented in Figure 5., whereas the spectral features, such as peak position (λ_{ex} / λ_{em}) and fluorescence intensity values, are listed in Table 2. The two Rayleigh scattering peaks, *i.e.*, the first-order scattering peak (peak 'a'; $\lambda_{ex} = \lambda_{em}$) and the second-order scattering peak (peak 'b'; $2\lambda_{ex} = \lambda_{em}$), are frequently detected in the proteins' 3-D fluorescence spectra.[50,51] The major peaks, peak '1' (λ_{ex} = 280 nm) and peak '2' (λ_{ex} = 230 nm), represented the fluorescence characteristics of Trp and Tyr residues of HSA. Presence of REG in the HSA solution ([REG] : [HSA] = 2 : 1) reduced the intensity values of two peaks, showing a drop of ~28 % for peak '1' and ~59 % for peak '2' (Table 2). The decrease in the fluorescence intensity of peaks '1' and '2' consequent to REG addition (Figure 5.; Table 2.) reflected changes in the Trp and Tyr microenvironment, which can be regarded as due to the binding of REG to HSA. This conclusion seems justifiable as Tyr residues are scattered in all domains of HSA, being 7, 7 and 4 in domains I, II and III, respectively.[24] In contrast, the lone Trp residue is located near Sudlow's Site I.[9]

Influence of REG Binding on HSA Thermal Stability

The protein thermal stability was checked by monitoring the protein's fluorescence intensity with rising temperature without and upon the addition of REG. Figure 6. displays temperature-induced differences in the fluorescence intensity at 343 nm of the protein and REG–protein (2 : 1) mixture. The inclusion of REG reduced the intensity values, particularly at higher temperatures (318–353 K), compared

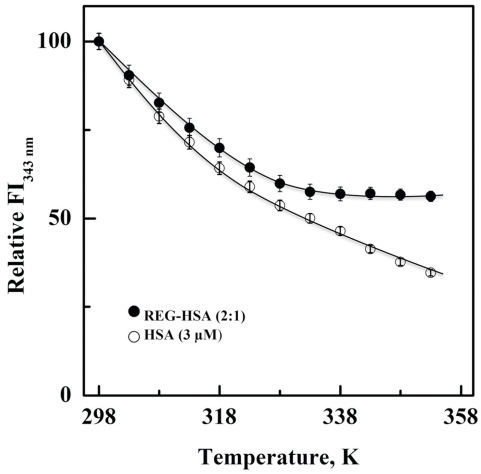

Figure 6. Plot displaying temperature-induced differences in the $FI_{343\ nm}$ value of pure HSA (3 μmol dm^{-3}) and 2:1 REG–HSA mixture, as studied in PB 7.4 in the temperature range 298–353 K at regular increments of 5 K.

to the decline in its absence. The quantitative assessment of the $FI_{343\ nm}$ of HSA and REG–HSA mixture presented ~65 % and ~44 % loss in the fluorescence intensity, respectively, at 353 K. Enhancement in the $FI_{343\ nm}$ value of REG–protein mixture at the rising temperature suggested resistance against temperature stress. The noncovalent interactions due to REG–HSA complex formation might have added to the thermostability of HSA upon REG–HSA interaction.

Identification of the REG Binding Site in HSA

Many drugs exhibit higher binding affinity towards either Sudlow's Site I or Sudlow's Site II. Therefore, these two well-characterized ligand binding sites of HSA were targeted to uncover the preferable REG binding locus on HSA.[9,50] Competitive ligand displacement experiments were performed using site-specific marker ligands such as PBZ and WFN for Site I and DZM for Site II.[9]

The fluorescence spectra of [WFN] : [protein] = 1 : 1 mixture without and with the inclusion of increasing REG concentrations are displayed in Figure 7A. WFN in protein-bound form produced a fluorescence spectrum in the wavelength range 360-480 nm when excited at 335 nm (spectrum 1). However, the fluorescence intensity of protein-bound WFN at the λ_{em} peak (383 nm) progressively quenched upon successive addition of REG (Figure 7A.). It is worth mentioning that except for WFN, pure HSA or REG and REG-HSA mixture did not generate any considerable fluorescence signal throughout the selected wavelength range. About a 40 % drop in the value at $FI_{383\ nm}$ was seen at the REG/HSA molar ratio of 2 : 1 (inset of Figure 7A.). Such decline in the fluorescence signal of protein-bound WFN reflected displacement of WFN from Sudlow's Site I due to its competition with REG.

To corroborate the findings drawn from the above experiment, the protein and other protein-bound site markers were also titrated with increasing concentrations of REG. Titration results of HSA and [PBZ]/[DZM] : [HSA] = 1 : 1 mixtures with REG are presented in Figure 7B. A gradual drop in the $FI_{343\ nm}$ value was evident upon rising REG/HSA molar ratios in both the protein and PBZ/DZM–HSA

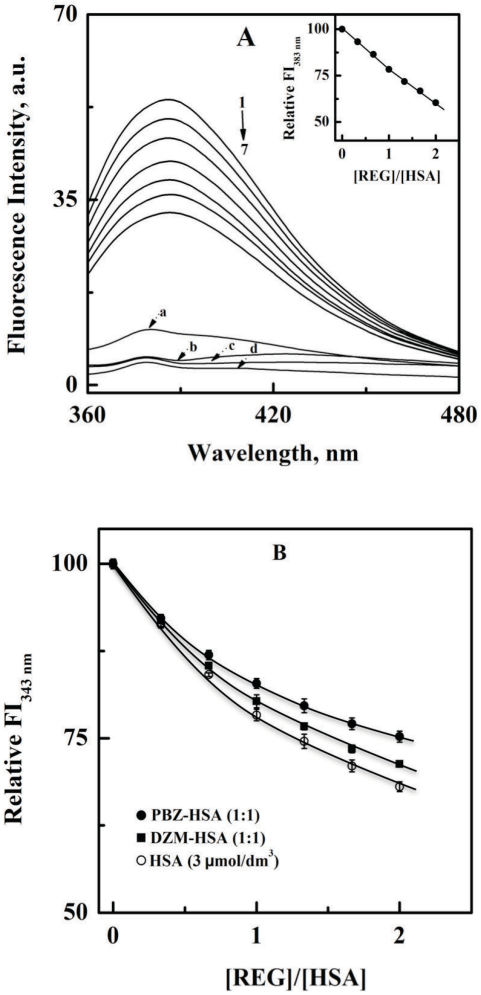

Figure 7. (A) Plot showing quenching of the fluorescence spectrum of 1 : 1 WFN–HSA (3 μmol dm^{-3} each) mixture (spectrum 1) upon inclusion of rising concentrations (1, 2, 3, 4,5 and 6 μmol dm^{-3}) of REG (spectra 2–7). The spectra of 3 μmol dm^{-3} WFN, 3 μmol dm^{-3} HSA, 2 : 1 REG–HSA mixture and 6 μmol dm^{-3} REG are also included as 'a', 'b', 'c' and 'd', respectively. The inset depicts the decline in the fluorescence intensity of the WFN–HSA complex at 383 nm ($FI_{383\ nm}$) with growing REG/HSA molar ratio. These spectra were scanned in PB 7.4 at 298 K, using λ_{ex} of 335 nm. (B) REG-induced quenching in the $FI_{343\ nm}$ of HSA (3 μmol dm^{-3}) and 1 : 1 PBZ/DZM–HSA mixtures with rising REG/HSA molar ratio, as obtained in PB 7.4 at 298 K, using λ_{ex} of 295 nm.

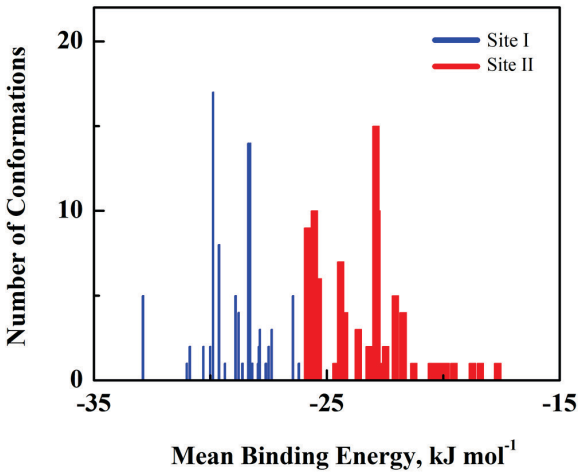

Figure 8. Cluster analysis (RMSD = 2.0 Å) of the docking results of REG-HSA complex, as made with a total of 100 docking runs for two binding sites, *i.e.,* Site I and Site II of HSA (1BM0).

mixtures. The decrease in the $FI_{343\ nm}$ value was relatively lower for the PBZ–HSA mixture compared to pure HSA and DZM–HSA systems. The differences in the $FI_{343\ nm}$ values suggested a competition between REG and PBZ for the mutual binding site, *i.e.*, Sudlow's Site I (subdomain IIA).

The above information pointed out Sudlow's Site I as the preferred REG binding site on the protein, which was well endorsed by our molecular docking analysis.

Molecular Docking Results of the REG–HSA System

The molecular docking assessment was performed to anticipate the REG binding site on HSA and substantiate the findings of the competitive drug displacement experiments discussed earlier. Two primary ligand binding sites, *i.e.*, Site I and Site II, were selected as the prime target for the docking analysis. The binding energy and interactions of the formed complexes were evaluated. The most populated cluster with 17 members for HSA Site I had mean binding energy of – 29.9 kJ mol^{-1}, whereas there were 15 members in the most populated cluster for HSA Site II with a mean binding energy of – 22.9 kJ mol^{-1} (Figure 8.). The lower (more negative) binding energy value of a ligand-protein complex would suggest a higher probability of forming a ligand-protein complex at the binding site.[53] REG complexed with HSA Site I had a lower binding energy value (– 33.3 kJ mol^{-1}) than that of the complex of REG with HSA Site II (– 27.2 kJ mol^{-1}) (Table 3.). The mean binding energy and the lowest binding energy results indicated that REG favoured binding to Site I in HSA. In addition, the hydrogen bonds, the hydrophobic interactions, and the polar interactions for the two complexes with the lowest binding energy were also assessed. The visualized representations are shown in Figures 9. and 10. For HSA Site I, two amino acid residues (Tyr150 and Arg257) participated in hydrogen bond formation (Figure 9B), while 15 residues (Lys195, Lys199, Trp214, Arg218, Leu219, Arg222, Leu234, Leu238,

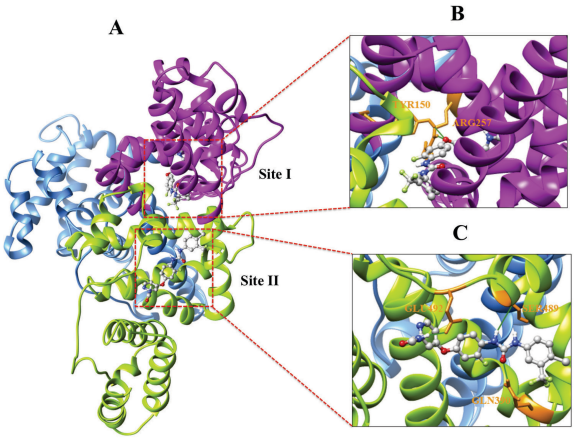

Figure 9. (A) The binding orientation of REG (represented in ball and stick) on Sudlow's Site I and Site II of HSA. The domains of HSA are coloured pink (domain I), blue (domain II), and green (domain III). The zoomed-in images show the hydrogen bonds (green lines) generated between the HSA residues (represented in the yellow stick) and REG at Sudlow's Site I (B) and Site II (C) of HSA.

Table 3. The lowest binding energy values and anticipated hydrogen bonds formed between atoms of amino acid residues of HSA (1BM0) and REG at binding Site I and Site II, as attained from the molecular docking analysis.

HSA binding sites	Lowest binding energy / kJ mol^{-1}	HSA residue: atom	REG atom	Distance / Å
Site I	– 33.3	Tyr-150: HH	O	2.31
		Arg-257: HE	O	2.13
Site II	– 27.2	Gln-390: HE22	O	2.37
		Ser-489: O	H	2.28
		Glu-492: OE2	H	2.03

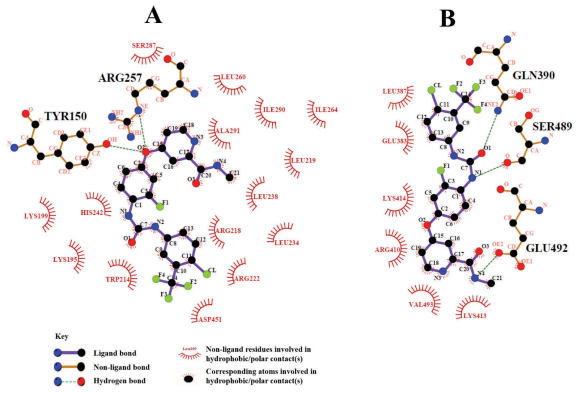

Figure 10. LigPlot+ maps present the hydrophobic and polar interactions between REG atoms and the protein's amino acid residues at Sites I (A) and II (B).

Leu260, His242, Ile264, Ile290, Ser287, Ala291 and Asp451) were involved in hydrophobic and polar interactions (Figure 10A.). On the contrary, for HSA Site II, three amino acid residues (Gln390, Ser489 and Glu492) were engaged in hydrogen bond formation (Figure 9C.), while six residues (Glu383, Leu387, Arg410, Lys413, Lys414 and Val493) assisted in hydrophobic and polar interactions (Figure 10B.). Our previous docking studies involving various ligands with HSA revealed that the hydrophobic and van der Waals interactions, along with hydrogen bonds, were responsible for the complex formation.[54,55] These interactions were also realized between REG and the amino acid residues in the protein's binding site.[53] Based on the more favourable binding energy and numerous interactions (hydrophobic and polar interactions, hydrogen bonds) between REG and HSA Site I, this type of complex was selected for further molecular dynamics (MD) simulation analysis.

Molecular Dynamics Simulations Analysis of the REG–HSA System

Molecular Dynamics (MD) simulation for a 50 ns time scale was performed to determine the stability and study the molecular interactions of the HSA Site I and REG complex. During the MD simulation, the average pressure and temperature were maintained at 0.96 bar and 299.99 K, respectively. As shown in Figure 11A., the ligand remains intact to the protein throughout the 50 ns MD simulation. Furthermore, the system's average total energy (–1,584,440 kJ mol^{-1}) was low.[56] Figure 11B. shows the root mean square deviation (RMSD) plot for REG–HSA complex (blue), HSA Carbon-alpha (Cα) atoms (green), and REG (purple). The RMSD values of the complex and HSA showed that the entire MD trajectory reached an equilibration state after 10 ns. The RMSD values of REG also maintained a stable trend. The RMSD values for the complex, HSA, and REG did not exceed 0.35 nm, indicating that the structures did not deform during the MD simulation.[57] The flexibility of the HSA residues can be seen in Figure 11C. The root mean square fluctuation (RMSF) plot demonstrated higher fluctuations for the loop regions and lower fluctuations for the secondary structures (alpha helices). Loop regions were expected to produce higher fluctuations due to their highly flexible nature.[58] Contrarily, having lower fluctuations meant that the alpha-helices remained compact throughout the MD simulation.[59]

Furthermore, for studying the compactness of the complex, the radius of gyration (R_g) plot was generated, which exhibited lesser fluctuations around ~2.70 nm (Figure 11D.). The hydrogen bond plot was produced to show the interactions between REG and HSA Site I. However, it can be observed that after 3 ns, there was no H-bond formation (Figure 11E.) due to the hydrophobic nature of the HSA Site I, which could hinder the formation of H-bonds.[60] The HSA Site I residues interacting with REG could be buried more profound into the binding site and produce weaker H-bonds, which were not detected.[61] Despite lacking H-bond formation, REG did not dislodge from the HSA Site I

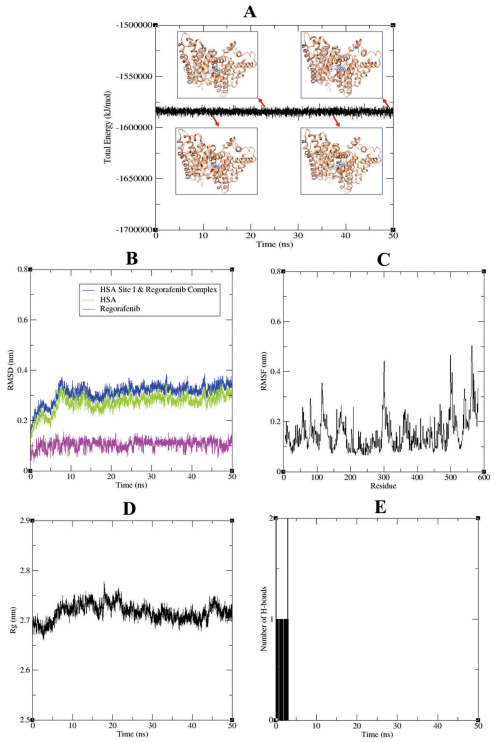

Figure 11. MD simulation energy analysis of the REG–HSA system, as acquired throughout the 50 ns MD simulations. Plots showing (A) the system's average total energy throughout the 50 ns, (B) RMSD plot for HSA Site I and REG complex (blue), HSA Cα atoms (green), and REG (purple), (C) RMSF for HSA, (D) computed radius of gyration (R_g) of HSA, and (E) hydrogen bonds formation between REG and HSA.

(Figure 11A.). Other interactions, such as hydrophobic and van der Waals interactions (as shown in Figure 10.), could be a possible contributor towards the complex formation. The above MD simulation analysis supported the experimental observation that the HSA Site I was mainly involved in REG binding.

CONCLUSION

The fluorescence and the UV-Vis absorption spectral results suggested the complexation between REG and the protein, involving intermediate binding affinity. *In vitro* and *in silico* analyses projected that hydrophobic interactions, van der Waals forces and hydrogen bonds participated in stabilizing the REG–HSA complex. Examination of 3-D fluorescence spectra detected the variations in the microenvironment around Trp and Tyr residues of HSA upon binding to REG. The preferred REG binding site was identified in the vicinity of Sudlow's Site I in HSA, according to the competitive drug displacement findings and molecular docking analysis. These detailed results provide valuable information about the pharmacokinetics of REG in human circulation, as drug-protein interaction increases the drug's efficacy, solubility and *in vivo* half-life while defending its elimination from the body and reducing its toxicity.

Acknowledgements. The Universiti Malaya Frontier Research Grant (FRG) 2017 (FG025-17AFR) financially supported this work. The authors thank the Dean, Faculty of Science, and the Head, Institute of Biological Sciences, Universiti Malaya, for providing the necessary facilities.

Conflict of interest. The authors declare that they have no known competing financial interests or personal relationships that could have appeared to influence the work reported in this paper.

Supplementary Information. Supporting information to the paper is attached to the electronic version of the article at: https://doi.org/10.5562/cca3922.

PDF files with attached documents are best viewed with Adobe Acrobat Reader which is free and can be downloaded from Adobe's web site.

REFERENCES

[1] G. D. Demetri, P. Reichardt, Y. K. Kang, J. Y. Blay, P. Rutkowski, H. Gelderblom, P. Hohenberger, M. Leahy, M. V. Mehren, H. Joensuu, G. Badalamenti, M. Blackstein, A. L. Cesne, P. Schoffski, R. G. Maki, S. Bauer, B. B. Nguyen, J. Xu, T. Nishida, J. Chung, C. Kappeler, I. Kuss, D. Laurent, P. G. Casali, *The Lancet* **2013**, *381*, 295–302. https://doi.org/10.1016/S0140-6736(12)61857-1

[2] A. Grothey, E. V. Cutsem, A. Sobrero, S. Siena, A. Falcone, M. Ychou, Y. Humblet, O. Bouche, L. Mineur, C. Barone, A. Adenis, J. Tabernero, T. Yoshino, H.-J. Lenz, R. M. Goldberg, D. J. Sargent, F. Cihon, L. Cupit, A. Wagner, D. Laurent, *The Lancet* **2013**, *381*, 303–312. https://doi.org/10.1016/S0140-6736(12)61900-X

[3] D. Strumberg, M. E. Scheulen, B. Schultheis, H. Richly, A. Frost, M. Büchert, O. Christensen, M. Jeffers, R. Heinig, O. Boix, K. Mross, *Br. J. Cancer* **2012**, *106*, 1722–1727. https://doi.org/10.1038/bjc.2012.153

[4] S. M. Wilhelm, J. Dumas, L. Adnane, M. Lynch, C. A. Carter, G. Schütz, K.-H. Thierauch, D. Zopf, *Int. J. Cancer* **2011**, *129*, 245–255. https://doi.org/10.1002/ijc.25864

[5] T. J. Ettrich, T. Seufferlein, *Small Molecules in Oncology*. Springer, Heidelberg, **2014**, p. 185.

[6] E. Daudigeos-Dubus, L. L. Dret, C. Lanvers-Kaminsky, O. Bawa, P. Opolon, A. Vievard, I. Villa, M. Pages, J. Bosq, G. Vassal, D. Zopf, B. Geoerger, *PLoS ONE* **2015**, *10*, e0142612. https://doi.org/10.1371/journal.pone.0142612

[7] H. Arai, F. Battaglin, J. Wang, J. H. Lo, S. Soni, W. Zhang, H. J. Lenz, *Cancer Treat. Rev.* **2019**, *81*, 101912. https://doi.org/10.1016/j.ctrv.2019.101912

[8] U. Kragh-Hansen, *Biochim. Biophys. Acta* **2013**, *1830*, 5535–5544. https://doi.org/10.1016/j.bbagen.2013.03.015

[9] U. Kragh-Hansen, V. T. G. Chuang, M. Otagiri, *Biol. Pharm. Bull.* **2002**, *25*, 695–704. https://doi.org/10.1248/bpb.25.695

[10] H. Mahaki, M. Memarpoor-Yazdi, J. Chamani, M. R. Saberi, *J. Lumin.* **2013**, *134*, 758–771. https://doi.org/10.1016/j.jlumin.2012.06.051

[11] K. Yamasaki, V. T. G. Chuang, T. Maruyama, M. Otagiri, *Biochim. Biophys. Acta – Gen Subj.* **2013**, *1830*, 5435–5443. https://doi.org/10.1016/j.bbagen.2013.05.005

[12] H. Tanzadehpanah, H. Mahaki, M. Moradi, S. Afshar, N. H. Moghadam, S. Salehzadeh, R. Najafi, R. Amini, M. Saidijam, *Protein Pept. Lett.* **2020**, *27*, 1–14. https://doi.org/10.2174/0929866527666200921164536

[13] L. Painter, M. M. Harding, P. J. Beeby, *J. Chem. Soc. Perkin Trans. (1)* **1998**, *1*, 3041–3044. https://doi.org/10.1039/a803429j

[14] S. M. Twine, M. G. Gore, P. Morton, B. C. Fish, A. G. Lee, J. M. East, *Arch. Biochem. Biophys.* **2003**, *414*, 83–90. https://doi.org/10.1016/S0003-9861(03)00173-5

[15] S. Tayyab, S. E. Sam, M. Z. Kabir, N. F. W. Ridzwan, S. B. Mohamad, *Spectrochim. Acta A. Mol. Biomol. Spectrosc.* **2019**, *214*, 199–206. https://doi.org/10.1016/j.saa.2019.02.028

[16] K. A. Musa, T. Ning, S. B. Mohamad, S. Tayyab, *J. Mol. Liq.* **2020**, *311*, 113270. https://doi.org/10.1016/j.molliq.2020.113270
[17] J. R. Lakowicz, *Principles of Fluorescence Spectroscopy*, Third ed., Springer, New York, **2006**.
[18] N. Tayeh, T. Rungassamy, J. R. Albani, *J. Pharm. Biomed. Anal.* **2009**, *50*, 107–116. https://doi.org/10.1016/j.jpba.2009.03.015
[19] M. Z. Kabir, Z. Benbekhti, N. F. Ridzwan, R. Merrouche, N. Bouras, S. B. Mohamad, S. Tayyab, *J. Mol. Liq.* **2020**, *303*, 112648. https://doi.org/10.1016/j.molliq.2020.112648
[20] S. Sugio, A. Kashima, S. Mochizuki, M. Noda, K. Kobayashi, *Protein Eng.* **1999**, *12*, 439–446. https://doi.org/10.1093/protein/12.6.439
[21] S. Kim, J. Chen, T. Cheng, A. Gindulyte, J. He, S. He, Q. Li, B. A. Shoemaker, P. A. Thiessen, B. Yu, L. Zaslavsky, J. Zhang, E. V. Bolton, *Nucleic Acids Res.* **2019**, *47*, 1102–1109. https://doi.org/10.1093/nar/gky1033
[22] N. M. O'Boyle, M. Banck, C. A. James, C. Morley, T. Vandermeersch, G. R. Hutchison, *J. Cheminform.* **2011**, *3*, 33–46. https://doi.org/10.1186/1758-2946-3-33
[23] G. M. Morris, R. Huey, W. Lindstrom, M. F. Sanner, R. K. Belew, D. S. Goodsell, A. J. Olson, *J. Comput. Chem.* **2009,** *30*, 2785–2791. https://doi.org/10.1002/ jcc.21256
[24] J. Fuhrmann, A. Rurainski, H. P. Lenhof, D. Neumann, *J. Comput. Chem.* **2010**, *31*, 1911–1918. https://doi.org/10.1002/jcc.21478
[25] E. F. Pettersen, T. D. Goddard, C. C. Huang, G. S. Couch, D. M. Greenblatt, E. C. Meng, T. E. Ferrin, *J. Comput. Chem.* **2004**, *25*, 1605–1612. https://doi.org/10.1002/jcc.20084
[26] R. A. Laskowski, M. B. Swindells, *J. Chem. Inf. Model.* **2011**, *51*, 2778–2786. https://doi.org/10.1021/ ci200227u
[27] M. J. Abraham, T. Murtola, R. Schulz, S. Páll, J. C. Smith, B. Hess, E. Lindahl, *SoftwareX* **2015**, *1*, 19–25. https://doi.org/10.1016/j.softx.2015.06.001
[28] J. B. Klauda, R. M. Venable, J. A. Freites, J. W. O'Connor, D. J. Tobias, C. Mondragon-Ramirez, I. Vorobyov, A. D. Mackerell, Jr, R. W. Pastor, *J. Phys. Chem. B.* **2010**, *114*, 7830–7843. https://doi.org/10.1021/jp101759q
[29] V. Zoete, M. A. Cuendet, A. Grosdidier, O. Michielin, *J. Comput. Chem.* **2011**, *32*, 2359–2368. https://doi.org/10.1002/jcc.21816
[30] W. L. Jorgensen, J. Chandrasekhar, J. D. Madura, R. W. Impey, M. L. Klein, *J. Chem. Phys.* **1983**, *79*, 926–935. https://doi.org/10.1063/1.445869
[31] S. E. Feller, Y. Zhang, R. W. Pastor, B. R. Brooks, *J. Chem. Phys.* **1995**, *103*, 4613–4621. https://doi.org/10.1063/1.470648
[32] T. Darden, D. York, L. Pedersen, *J. Chem. Phys.* **1993**, *98*, 10089–10092. https://doi.org/10.1063/1.464397
[33] B. Hess, H. Bekker, H. J. Berendsen, J. G. Fraaije, *J. Comput. Chem.* **1997**, *18*, 1463–1472. https://doi.org/10.1002/(SICI)1096-987X(199709)18:12<1463::AID-JCC4>3.0.CO;2-H
[34] P. J. Turner, *XMGRACE, Version 5.1.19.* **2005**, Center for Coastal and Land-Margin Research, Oregon Graduate Institute of Science and Technology, Beaverton.
[35] Y. Hui, X. Xue, Z. Xuesong, W. Yan, *Adv. Eng. Res.* **2015**, *15*, 224–233. https://doi.org/10.2991/icadme-15.2015.46
[36] N. C. Khanna, M. Tokuda, D. M. Waisman, *J. Biol. Chem.* **1986**, *261*, 8883–8887. https://doi.org/10.1016/S0021-9258(19)84464-2
[37] M. Yang, D. Shi, Y. Wang, A. G. Ebadi, M. Toughani, *Int. J. Pept. Res. Ther.* **2021**, *27*, 421-431. https://doi.org/10.1007/s10989-020-10096-6
[38] C. Wang, D. Shi, F. Zhang, X. Yu, G. Lin, Z. Zhou, *Spectrochim. Acta A. Mol. Biomol. Spectrosc.* ***2020***, *234*, 118245. https://doi.org/10.1016/j.saa.2020.118245
[39] W. R. Ware, *J. Phys. Chem.* **1962**, *66*, 455–458. https://doi.org/10.1021/j100809a020
[40] S. R. Feroz, S. B. Mohamad, Z. S. D. Bakri, S. N. A. Malek, S. Tayyab, *PLoS ONE* **2013**, *8*, e76067. https://doi.org/10.1371/journal. pone.0076067
[41] S. Kandandapani, M. Z. Kabir, N. F. W. Ridzwan, S. B. Mohamad, S. Tayyab, *J. Biomol. Struct. Dyn.* **2021**, *19*, 1–12. https://doi.org/10.1080/07391102.2021.1911850
[42] M. S. Nair, *J. Photochem. Photobiol. B. Biol.* **2015**, *149*, 58–67. https://doi.org/10.1016/j.jphotobiol.2015.05.001
[43] Q. Wang, C. R. Huang, M. Jiang, Y. Y. Zhu, J. Wang, J. Chen, S. H. Shi, *Spectrochim. Acta A. Mol. Biomol. Spectrosc.* **2016**, *156*, 155–163. https://doi.org/10.1016/j.saa.2015.12.003
[44] V. Sinisi, C. Forzato, N. Cefarin, L. Navarini, F. Berti, *Food Chem.* **2015**, *168*, 332–340. https://doi.org/10.1016/j.foodchem.2014.07.080
[45] L. Yuan, M. Liu, G. Liu, D. Li, Z. Wang, B. Wang, J. Han, M. Zhang, *Spectrochim. Acta A. Mol. Biomol. Spectrosc.* **2017**, *173*, 584–592. https://doi.org/10.1016/j.saa.2016.10.023
[46] L. Trnkova, I. Bousova, V. Stankova, J. Drsata, *J. Mol. Struct.* **2011**, *985*, 243–250. https://doi.org/10.1016/j.molstruc.2010.11.001
[47] B. Rastegari, H. R. Karbalaei-Heidari, R. Yousefi, S. Zeinali, M. Nabavizadeh, *Bioorg. Med. Chem.* **2016**, *24*, 1504–1512.

https://doi.org/10.1016/j.bmc.2016.02.020
[48] B. Sandhya, A. H. Hedge, J. Seetharamappa, *Mol. Biol. Rep.* **2013**, *40*, 3817–3827. https://doi.org/10.1007/s11033-012-2460-8
[49] D. P. Ross, S. Subramanian, *Biochemistry* **1981**, *20*, 3096–3102. https://doi.org/10.1021/bi00514a017
[50] G. Sudlow, D. J. Birkett, D. N. Wade, *Mol. Pharmacol.* **1975**, *11*, 824–832.
[51] B. K. Bozoğlan, S. Tunç, O. Duman, *J. Lumin.* **2014**, *155*, 198–204. https://doi.org/10.1016/j.jlumin.2014.06.032
[52] X. Chen, K. Qian, Q. Chen, *Eur. J. Med. Chem.* **2015**, *93*, 492–500. https://doi.org/10.1016/j.ejmech.2015.02.025
[53] S. M. Auwal, N. Z. Abidin, M. Zarei, C. P. Tan, N. Saari, *PLoS ONE* **2019**, *14*, e0197644. https://doi.org/10.1371/journal.pone.0197644
[54] M. Z. Kabir, S. B. Mohamad, N. Omer, Y. M. Choo, S. Tayyab, *Biointerface Res. Appl. Chem.* **2022**, *12*, 5296–5302. https://doi.org/10.33263/BRIAC124.52965302
[55] A. A. A. Halim, N. F. W. Ridzwan, S. B. Mohamad, S. Tayyab, *Biointerface Res. Appl. Chem.* **2022**, *12*, 1520–1525. https://doi.org/10.33263/BRIAC122.15201525
[56] F. Sharif, A. M. Yunus, R. R. Saedudin, A. A. A. Hamid, S. Kasim, *Int. J. Integr. Eng.* **2018**, *10*, 119–127. https://penerbit.uthm.edu.my/ojs/index.php/ijie/article/view/2771
[57] J. Zhang, L. Zhang, Y. Xu, S. Jiang, Y. Shao, *PLoS ONE* **2018**, *13*, e0196651. https://doi.org/10.1371/journal.pone.0196651
[58] L. Piao, Z. Chen, Q. Li, R. Liu, W. Song, R. Kong, S. Chang, *Int. J. Mol. Sci.* **2019**, *20*, 224–240. https://doi.org/10.3390/ijms20010224
[59] V. Nemaysh, P. M. Luthra, *RSC Adv.* **2017**, *7*, 37612–37626. https://doi.org/10.1039/c7ra01305a
[60] D. Wu, J. Wang, D. Liu, Y. Zhang, X. Hu, *Sci. Rep.* **2019**, *9*, 1–8. https://doi.org/10.1038/s41598-018-38240-9
[61] T. M. Musyoka, A. M. Kanzi, K. A. Lobb, O. T. Bishop, *Sci. Rep.* **2016**, *6*, 23690. https://doi.org/10.1038/srep23690